

# THE X-RAY ZURICH ENVIRONMENTAL STUDY (X-ZENS). II. X-RAY OBSERVATIONS OF THE DIFFUSE INTRAGROUP MEDIUM IN GALAXY GROUPS

FRANCESCO MINIATI<sup>1</sup>, ALEXIS FINOGENOV<sup>2</sup>, JOHN D. SILVERMAN<sup>3</sup>, MARCELLA CAROLLO<sup>1</sup>, ANNA CIBINEL<sup>4</sup>, SIMON J. LILLY<sup>1</sup>, KEVIN SCHAWINSKI<sup>1</sup>

*Draft version July 30, 2021*

## ABSTRACT

We present the results of a pilot XMM-Newton and Chandra program aimed at studying the diffuse intragroup medium (DIM) of optically-selected nearby groups from the Zurich ENvironmental Study (ZENS) catalog. The groups are in a narrow mass range about  $10^{13} M_{\odot}$ , a mass scale at which the interplay between the DIM and the group member galaxies is still largely unprobed. X-ray emission from the DIM is detected in the energy band 0.5–2 keV with flux  $\leq 10^{-14}$  erg cm<sup>-2</sup> s<sup>-1</sup>, which is one order of magnitude fainter than for typical ROSAT groups (RASS). For many groups we set upper limits to the X-ray luminosity, indicating that the detections are likely probing the upper envelope of the X-ray emitting groups. We find evidence for our optically selected groups to be under-luminous with respect to predictions from X-ray scaling relations. X-ray mass determinations are in best agreement with those based on the member galaxies bulge luminosity, followed by their total optical luminosity and velocity dispersion. We measure a stellar mass fraction with a median value of about 1%, with a contribution from the most massive galaxies between 30 to 50 %. Optical and X-ray data give often complementary answers concerning the dynamical state of the groups, and are essential for a complete picture of the system. Extending this pilot program to a larger sample of groups is mandatory to unveil any imprint of interaction between member galaxies and DIM in halo potentials of key importance for environmentally-driven galactic evolution.

*Subject headings:* Cosmology – large-scale structure of universe – galaxies: groups: general – X-rays: galaxies: groups – methods: observational

## 1. INTRODUCTION

Galaxy groups in the mass range  $10^{13} - 10^{14} M_{\odot}$  are key structures in the cosmic fabric. Containing typically between a few to a few tens of member galaxies (Mulchaey et al. 2000, 2003), they are significantly more numerous than galaxy clusters, trace the filamentary components of the large scale structure (e.g. Eke et al. 2004) and are likely to contain a large fraction of the unaccounted cosmic baryons (Fukugita et al. 1998). Groups have historically been detected in the X-ray emission, typically extending on scales of a few hundred kpc, revealing a gas in a state of diffuse, ionized and metal rich plasma with temperature around one keV. The plasma emission mechanism is a combination of thermal bremsstrahlung and line emission, the latter more prominent in groups than in clusters of galaxies due to the lower plasma temperature. The detection of hot plasma bears witness to the fact that groups are not simply associations of galaxies by way of projection effects, but real physical systems, gravitationally bound and having undergone some degree of virialization.

Groups host about 50 to 70% of today's  $L^*$  galaxies (Eke et al. 2005), thus providing the environment most commonly experienced by the latter. The role and

impact of group environment on galaxies is therefore subject of detailed studies in both optical and X-ray surveys (e.g. Rasmussen et al. 2006; Weinmann et al. 2006; Poggianti et al. 2008; McGee et al. 2011; Knobel et al. 2012; Giodini et al. 2012; Carollo et al. 2013, among the others). Theoretical models indicate that groups can be instrumental in triggering processes that accelerate galaxy evolution. For example, the in-spiral timescale of dynamical friction varies in proportion to  $\sigma^3/\rho$ , where  $\sigma$  and  $\rho$  are the halo velocity dispersion and density, respectively. Thus, compared to the field and galaxy clusters, galaxy tidal interactions due to close encounters (harassment) and mergers take place on a cosmologically short timescale in groups, characterized by significant over-density and relatively low velocity dispersion (Barnes et al. 1990). Such galaxy-galaxy interactions induce dynamical instabilities (Mayer et al. 2001), plausibly allow for the fueling of central super-massive black holes (SMBHs, Barnes and Hernquist 1991; Barnes et al. 2002; Mihos 2003) and are likely to play a major role in the evolution of massive galaxies within the group environment (McIntosh et al. 2008; Feldmann et al. 2010; Robotham et al. 2013). In addition, gas dynamical interactions with the diffuse intragroup medium (DIM), such as ram-pressure stripping of cold gas in the stellar disk and/or strangulation of the baryonic supply from the halo reservoir, can severely reduce the gas available for star formation and feedback process even in relatively low density environment (Kawata et al. 2008; McCarthy et al. 2008), possibly leading to the observed satellite quenching in groups (e.g., van den Bosch et al. 2008; Skibba 2009; Peng et al.

<sup>1</sup> Physics Department, Wolfgang-Pauli-Strasse 27, ETH-Zürich, CH-8093, Zürich, Switzerland; fm@phys.ethz.ch

<sup>2</sup> Department of Physics, Gustaf Hållströmin katu 2a, FI-00014, University of Helsinki, Finland

<sup>3</sup> Institute for the Physics and Mathematics of the Universe (IPMU), University of Tokyo, Kashiwanoha 5-1-5, Kashiwa-shi, Chiba 277-8568, Japan

<sup>4</sup> CEA Saclay, DSM/Irfu/Sérvise d'Astrophysique, Orme des Merisiers, F-91191 Gif-sur-Yvette Cedex, France

2012; Wetzel et al. 2013; Carollo et al. 2014; Tal et al. 2014).

The group mass sets an important scale, one at which the processes of large scale structure formation and galaxy formation meet. In fact, the thermodynamic properties of the DIM deviate substantially from scaling relations obeyed by massive clusters, an indication that processes other than gravity and (magneto-) hydrodynamics affect in an important way the gas energetics at this mass scale. Particular attention has been devoted to the study of gas entropy, because it is conserved during adiabatic processes and changes only according to the net amount of thermal energy either absorbed or released by the gas. Gas entropy in groups appears in clear excess with respect to the expected value from the scaling relations obeyed by clusters, (Ponman et al. 1999; Lloyd-Davis et al. 2000; Finoguenov et al. 2001; Ponman et al. 2003; Madhavi et al. 2005; Prat et al. 2010), a fact ascribed, at least in part, to energetic feedback from galaxy formation processes (e.g., Voit et al. 2002; Cavaliere et al. 1998; Borgani et al. 2005; McCarthy et al. 2010; Giodini et al. 2010). In fact, due to the group’s shallow potential well and corresponding low virial temperature, the energy released by past star formation and AGN activity leaves a distinct footprint on the thermodynamic properties of the DIM. In addition, the DIM appears highly enriched with significant amounts of metals, most likely transported there from the parent galaxy through stellar winds (Rasmussen and Ponman 2009; McCarthy et al. 2010). Winds associated with metal transition lines observed at redshift  $z \sim 1$  appear to be strongly magnetized (Bernet et al. 2008, 2010, 2012), so the DIM is likely to be significantly magnetized as well, in addition to being metal rich.

The above interplay between galaxies and DIM is important because it affects the observational properties of X-ray groups as well as those of galaxies. Its study is important in shedding light on the origin of the observed physical properties of the DIM, including amongst others, the radial profile of thermodynamic quantities such as entropy, temperature, and their dependence with virial mass (or any of its proxies). Likewise, the feedback processes described above, are believed to play a crucial role in galaxy evolution. In particular current models suggest that the growth of galaxies is intimately related to the growth of their black holes, and that AGN activity is key in preventing excessive cooling in massive galaxy halos (Bower et al. 2006; Croton et al. 2006; Bower et al. 2008).

From an observational point of view, the study of the interplay between galaxies and the DIM remains incomplete for two basic reasons. First, it is now well known that groups are a heterogeneous class, spanning a wide range in dynamical state (Mulchaey et al. 2000) and X-ray emission (Eckmiller et al. 2012). Because X-ray observations provides the most straightforward way for identifying groups, X-ray selected group samples are traditionally the best studied (e.g., Heldson and Ponman 2000; Finoguenov et al. 2001; Madhavi et al. 2005; Osmond and Ponman 2004; Rasmussen and Ponman 2007), and have delivered many important results. However, dynamically relaxed groups tend to be more X-ray bright, which raises an important and well appreciated

issue concerning the *representative* character of X-ray selected group samples. At cluster scales, several studies have indeed shown that the X-ray properties of optically-selected galaxy clusters differ substantially from those of the X-ray-selected structures (Donahue et al. 2002; Gilbank et al. 2004; Lubin et al. 2004; Popesso et al. 2007). With the advent of large spectroscopic surveys, e.g., the SDSS (York et al. 2000) and the 2dFGRS (Colless et al. 2001), it has become possible to identify also group-sized structures spectroscopically, i.e. through the identification of their member galaxies. Pioneering studies on a few systems have demonstrated the existence, also at the mass scales of groups, of less relaxed structures with low X-ray emissivity (Mulchaey et al. 2000; Rasmussen et al. 2006) that were missed in shallow X-ray surveys (RASS).

As for the second reason for the above incompleteness, studying galaxy groups up to now has been limited by the lack of accurate information about the properties of the galaxy-members together with the X-ray data. It is now clear, however, that in view of the rich variety of properties of galaxies observed at fixed group mass scale as a function of galaxy mass and of rank within the groups as central or satellite (Weinmann et al. 2006, 2008; Carollo et al. 2013; Carollo et al. 2014), this information is essential in order to elucidate the relation between group environment and the evolution of the member-galaxies.

Earlier efforts to study at X-ray representative samples of groups based on optical selection of member galaxies (Mahdavi et al. 1997, 2000; Burns et al. 1996; Ebeling et al. 1994; Ponman et al. 1996), have been mostly based, however, on shallow exposure RASS data and/or on limited information about the physical properties member galaxies. More recently, the Complete Local Group Sample (CLOGS; O’Sullivan et al. 2014) project is attempting to produce the first statistically complete survey of galaxy groups observed in the X-ray, optical and radio wavebands, which should greatly contribute to address the scientific questions raised above. Using a complementary approach, we have also started the Zurich ENvironmental Study (ZENS; Carollo et al. 2013; Cibinel et al. 2013a,b; Carollo et al. 2014), a program to build a representative sample of galaxy groups, unbiased with respect to dynamical conditions, with multi-wavelength coverage, and with fully determined properties of the member galaxies. The aim of our program is to study the environmental impact on the evolution of galaxies including, amongst others, the interplay between galaxy formation and DIM. The ZENS project, described in more detail in Sec. 2, differs in several respects from CLOG, which is also briefly discussed there for comparison.

In this paper we report on initial efforts to study the DIM with X-ray observations of ZENS groups. In particular we present data taken during the past few years with the XMM-Newton and Chandra telescopes on a subsample of ZENS groups. In this paper we focus on the diffuse X-ray emission while we report on the X-ray point-source detections in a companion paper (Silverman et al. 2014) aimed at investigating the role of AGN in the context of galaxy evolution in groups.

The XMM-Newton and Chandra observations, including the data analysis, are described in Sec. 3, while re-

sults concerning the diffuse X-ray emission are presented in Sec. 4. Results and conclusions are summarized in Sec. 5. In the following we assume a concordance  $\Lambda$ -CDM universe with parameters  $\Omega_m = 0.2792$ ,  $\Omega_b = 0.0462$ ,  $\Omega_\Lambda = 1 - \Omega_m$ , and Hubble constant  $H_0 = 70 \text{ km s}^{-1} \text{ Mpc}^{-1}$  (Komatsu et al. 2009).

## 2. THE ZURICH ENVIRONMENTAL STUDY (ZENS)

The ZENS project, including its design, the observations and the publicly available catalogue, and all environmental, structure and photometric measurements, are described in great details in the first three papers of the ZENS series (Carollo et al. 2013; Cibinel et al. 2013a,b, respectively Paper I, II and III), which we refer to, for further information. In the following we summarize aspects of the project which are relevant to this paper.

The ZENS data set consist of 141 groups, containing a total of 1630 galaxies, randomly extracted from the complete sample of groups of the 2dF Percolation–Inferred Galaxy Group catalog (Eke et al. 2004) (2PIGG), with at least five cataloged members and within the narrow redshift range,  $0.05 < z < 0.0585$ .

The groups are classified in terms of total mass, dynamical state (relaxed or unrelaxed) and location within the large scale structure environment, i.e., their proximity to massive clusters, filaments, or voids.

The ZENS galaxies have been fully characterised in terms of their stellar mass, star-formation activity, morphological/structural properties and central/satellite rank within the group. Resolved information such as size and strength of bars, color gradients, color maps as well as bulge and disks colors, stellar masses and structure properties have been also derived for our ZENS sample.

Among extant projects with similar objectives to ours, the already mentioned CLoGS is probably the one that comes closest in scope. In particular, the CLoGS project is aiming for a representative catalog of 53 local groups ( $z < 0.02$ ) with optical, radio and XMM or Chandra coverage. Our ZENS study differs from this projects in a number of important ways. The typical richness of CLoGS groups,  $N \gtrsim 20$ , is larger than the richness of the ZENS groups which have typically 10 members and thus bracket smaller halo masses. In addition, the CLoGS group are selected to have at least one luminous ( $L_B > 3 \times 10^{10} L_\odot$ ) early-type galaxy. While this likely ensures a group higher X-ray luminosity, it also likely introduces a bias in the probed sample towards more evolved/massive systems. Furthermore, while a basic morphological classification and integrated photometric information is also available in the HYPERLEDA catalog (Paturel et al. 2003) from which CLoGS is based, the ZENS dataset improves on such data by providing, as described above a comprehensive set of detailed properties for the whole galaxies, their bulges and disks.

## 3. OBSERVATIONS: DATA ACQUISITION, ANALYSIS AND SOURCE DETECTION

### 3.1. XMM-Newton

We have carried out XMM-Newton observations of ZENS groups during three consecutive observational programs (PI: Miniati, Prop. # 065530, Prop. #067448, Prop. #069374). As of today, 9 observations of groups have been performed. We have also retrieved data for 4

additional groups from the archive, for a set of 13 XMM-Newton observations of our ZENS groups.

Details of the observations are presented in Table 1, which reports: (1) the target name, (2) the observation ID, (3-4) the RA, DEC coordinates in J2000, (5) the group redshift, (6) the number of member galaxies, (7) the group mass inferred from the stellar mass, (8) XMM cycle of observation, (9) and the exposure time. The last column (10) contains notes about the observational data, in particular whether the observations suffered from “flares”.

The exposure times were estimated based on the expected X-ray luminosity of our targets, in the range  $3 \times 10^{40} < L_{0.5-2\text{keV}} / (\text{erg s}^{-1}) < 5 \times 10^{41}$  (Rasmussen and Ponman 2009). Detection of X-ray emission from groups is notoriously challenging. This is partly because X-ray luminosity scales with total mass of the emitting virialized system and becomes faint at the group mass scale. In addition, at such mass scale the X-ray luminosity-mass relation becomes characterized by considerable scatter (Eckmiller et al. 2012), causing uncertainties in the observational forecast. While this reminds us of the risk of observational biases in X-ray selected group samples, it also illustrates the difficulty associated with amending the problem.

Different exposure times in different observing cycles reflect different strategies underlying our successive proposals. In particular, in AO-9 we used long exposures as we aimed at measuring the thermodynamic properties of the intragroup medium. This, however, was achieved only for one of the three observed groups, which led us to revise our strategy in AO-10, and split the program in two separate steps: (1) first carry out a short exposure, to determine the group luminosity and then follow up with deeper observations bright enough groups that their thermodynamic properties can be determined with reasonable exposure times. This approach is made difficult, however, by the large incidence of flares, which can completely corrupt the data for short exposure times. Slightly longer exposures were therefore employed in AO-11.

The standard processing of the XMM observations included the screening for the flares, and making a composite images from all 3 detectors in the 0.5-2 and 2-7.5 keV bands, excluding the energies affected by the strong instrumental lines, as discussed in Finoguenov et al. (2007). We only used 0.5-2 keV images for detection extended emission (hard band is used to search for AGNs). We used the procedure of Finoguenov et al. (2007) with updates described in Bielby et al. (2010). We monitor the S/N ratio maps to control the quality of background removal. On several occasions hot MOS1 and MOS2 chips were removed. The flux of detected point sources was removed using PSF model of XMM before proceeding with extended source detection, as described in Finoguenov et al. (2009). In case of both Chandra and XMM observations we performed parallel analysis and compared the results, showing that estimated fluxes do not depend on the choice of the instrument.

Table 2 summarizes measurements of the X-ray emission from the diffuse intragroup medium, including upper limits for the non-detections. In particular it reports: (1)

target name, (2) total X-ray counts (extended and point sources including background), (3) background counts only, (4) counts due to point sources, (5) count extraction radius, (6) estimate of the total X-ray luminosity in the rest frame 0.1–2.4 keV band and, (7–9) corresponding virial mass, virial radius and temperature, using the scaling relation of (Leauthaud et al. 2010), (10) the source flux extrapolated to the virial radius, using the procedure outlined in (Finoguenov et al. 2007), (11) signal to noise ratio. Note that the formal statistical significance of the detected emission is larger than the reported flux significance. The results based on these measurements are discussed in Section 4.

### 3.2. *Chandra*

We also carried out *Chandra*/ACIS-I observations of 12 ZENS galaxy groups in Cycle 11 (Prog. # 11700688; 120 ksec). The observations were executed between September 2009 and October 2010. Each target is observed for 10 ksec, the main objective of these observations being the detection with at least 4 counts in the broad energy band 0.5–8 keV, of AGNs at  $z \sim 0.05$  down to a limiting luminosity of  $L_{(0.5-8 \text{ keV})} \sim 4 \times 10^{40} \text{ erg s}^{-1}$ . The field-of-view of ACIS-I ( $16.9' \times 16.9'$ ; CCDs #0–3) is sufficient to cover the sky area of these galaxy groups (size  $< 10'$ ). The target positions were chosen to avoid having galaxies falling within or near chip gaps; this was accomplished by adjusting the pointing location once the planned observation date was set thus the roll angle was known. In Table 3, we provide details on the individual exposures.

We employ a method to detect extended emission in our *Chandra* observations similar to that of a number of recent analysis (e.g., Cappelluti et al. 2012; Tanaka et al. 2012). We screen the event file by removing time intervals affected by flares, using the CIAO *lc\_clean* tool. Exposure maps (effective area versus sky position) are generated for each observation listed in Table 3 using *mkinstmap* and *mkexppmap*. To do so, we generate an instrument map (effective area versus detector position) in the 0.5–2 keV band using a model weighing scheme of a power law distribution with index of 1.7. For our purpose, the difference in the final exposure map when using either a power-law or thermal spectrum is negligible. Using the merged event files, we generate a combined image for each galaxy group in the 0.1–2.4 keV band.

The detection of diffuse emission requires the removal of point sources. To do so, we run *wavdetect* on the full image in the 0.1–2.4 keV band with a significance threshold of  $5 \times 10^{-6}$ . An input parameter of relevance is the encircled energy (39.3%) of the PSF at an energy of 1.5 keV. In addition, elliptical source regions of the output detections have a size of  $3\sigma$  of the PSF. After excising the photon events in these regions, an artificial background level is applied based on the level in a larger background region local to each source detection.

The background X-ray emission is estimated using the procedure of (Hickox & Markevitch 2006) that uses the particle background (of non-astrophysical origin) measured from the stowed position of ACIS (<http://cxc.cfa.harvard.edu/contrib/maxim/acisbg>) in the 9.5–12 keV energy range. We then scale this back-

ground map to match that expected in our observations by the ratio  $C_{data,9.5-12}/C_{stow,9.5-12}$  where  $C_{data}$  are the counts measured in the data while  $C_{stow}$  are the counts detected in the stowed position.

We run the 'wvdecomp' algorithm (Vikhlinin et al. 1998) on the data after subtracting the smoothed background maps, to search for extended sources on angular scales exceeding 30 arcseconds. In four cases, we detect emission and use a circular region with a radius matched to the extent of the emission for flux estimates. In cases where no emission is detected, we use a circular region with a 2–3 arcminute radius to determine an upper limit ( $2\sigma$ ) on the flux. We also measure a 'control' flux estimate in the source-free zone to refine the background subtraction. In cases of positive signal, we subtract it from the source emission with a scaling based on flux extraction area. We provide the following specific measurements of diffuse emission: (1) total counts, (2) background counts, (3) counts associated with embedded point sources, (4) the extrapolated flux of the source, using the procedure outlined in (Finoguenov et al. 2007), (5) estimate of the total X-ray luminosity in the rest frame 0.1–2.4 keV band and (6) a corresponding virial mass using the scaling relation of (Leauthaud et al. 2010). All results based on these measurements are discussed in Section 4.

In Table 4, we provide our measurements of the X-ray emission from the diffuse intragroup medium, that include upper limits for the non-detections. As for table relative to the XMM-*Newton* diffuse emission, the columns are as follows: (1) Name, (2) total X-ray counts (extended and point sources including background), (3) background counts only, (4) counts due to point sources, (5) count extraction radius, (6), luminosity, (7–9)  $M_{200}$ ,  $R_{200}$ , and X-ray temperature, respectively, based on the scaling relation of (Leauthaud et al. 2010), (10) source flux, and (11) significance of the detection of extended emission.

### 3.3. Selection Bias

Since the groups were selected to be within a specific mass range, the mean properties of the groups computed a posteriori as a function of the selection parameter are affected by a bias which need to be taken into account. The bias is due to the fact that systems below the mass threshold will still be selected due to statistical errors in the mass estimates, while systems above the mass threshold will not be selected due to mass underestimates. The effect is not symmetric across the low and high mass thresholds, because the mass function is a steep power-law. To amend for this effect we follow Vikhlinin et al. (2009) who suggested a way to estimate the bias factor for the purpose of optimizing the measurements of cluster scaling relations. In their approach the bias correction is specific to the individual values of the selection parameter  $M$ , and further depends the threshold,  $M_{th}$ , and dispersion,  $\sigma_M$ , of the latter as

$$\beta(M, \sigma_M) = \frac{\int_{M_{th}} (M - M_{th}) e^{-\frac{(M - M_{th})^2}{2\sigma_M^2}} dM}{\int_{M_{th}} e^{-\frac{(M - M_{th})^2}{2\sigma_M^2}} dM}. \quad (1)$$

The value of  $\sigma_M$  can be determined from the data and to first order is unbiased Vikhlinin et al. (2009). In Fig. 3 presented below we report bias corrected estimates of the group masses, assuming that  $\sigma_M$  corresponds to 50% of the mass measurements dispersions.

#### 4. RESULTS

Our X-ray observations of galaxy groups in ZENS with *XMM-Newton* and *Chandra* enable us to begin the construction of a sample selected without an obvious preference on their X-ray properties or dynamical state.

Of the 13 ZENS groups observed with *XMM-Newton* and listed in Table 1, one third have data that is severely affected by flares, and is thus not usable. This problem affected equally all observations with exposure time below 40 ksec. Of the remaining 9 groups with valid data, X-ray emission from the DIM was clearly detected in 5 cases, with a typical signal-to-noise 4–5, in addition to a two sigma detection. Group 2PIGG\_s1571 was an exception, with a signal-to-noise 46.87, much higher than for the other groups. The reminder of the X-ray observations includes a 1.8- $\sigma$  detection, a 2- $\sigma$  upper limits and an upper limit.

In comparison, of the 12 ZENS groups observed with *Chandra* and listed in Table 3, X-ray emission from the DIM was detected in a total of three cases. One of these cases corresponds to 2PIGG\_s1571 and, as for the case of *XMM-Newton*, it is detected with a high signal to noise. The flux measured by the two telescopes is consistent within the reported statistical error. The reminder of the X-ray observations include a 2- $\sigma$  detections, while the rest are upper limits.

These results reveal the presence of diffuse intragroup gas inside the shallow potential well of small scale groups with masses around  $10^{13} M_\odot$ . The X-ray emission is rather faint, with typical flux  $\leq 10^{-14}$  erg cm $^{-2}$  s $^{-1}$ , i.e. one order of magnitude fainter than typical ROSAT groups (RASS). In addition, for several groups we were able to measure upper limits, which implies that we are mostly probing the upper envelope of the X-ray emitting, optically selected ZENS groups. While this is likely due to diversity in X-ray luminosity of our groups at fixed mass, we cannot completely exclude that at least in some cases the effect is enhanced by uncertainties in the mass determination of the groups.

##### 4.1. X-ray vs Optical Images

In Fig. 1–2 we show examples of detection ( $S/N > 3$ ) of diffuse X-ray emission from ZENS groups, based on both *XMM-Newton* (2PIGG\_s1520, 2PIGG\_s1571, 2PIGG\_n1606) and *Chandra* (2PIGG\_s1571, 2PIGG\_n1320) observations. The contours indicate the surface brightness level of the X-ray emission on a log-scale and are superposed to optical i-band images of the respective group fields. Member galaxies are identified with a small circle, red in the case of satellites and blue for central galaxies. The latter correspond to galaxies with the highest stellar mass that also satisfy the following requirements: (1) to be close in position to the group centre and, (2) to move with respect to the group bulk at a velocity that is within one  $\sigma$  of the group velocity dispersion (see Carollo et al. 2013, for further details). In our ZENS work, we consistently assumed that the so-defined central galaxies identify the

centres of the groups. This approach differs from the original 2PIGG procedure of Eke et al. who computed and used, as group centre, a weighted average of the galaxy positions. Both these approaches were developed prior to any knowledge of the groups' X-ray emission, which now allows for a sensible consistency check of either optical definitions of centres, and between group properties determined with optical and with X-ray data. Of particular importance is the fact that the precise definition of a group centre also establishes the classification of its dynamical state.

We thus inspect the composite images in Fig. 1–2. Furthermore, Table 5 lists the difference between the 2PIGG optically-averaged and the X-ray centres of the groups (3rd column), as well as the distance of the group central galaxy to the 2PIGG (4th column) and X-ray (5th column) centres. The first three columns contain to the groups name and optical equatorial coordinates, while the last column indicates the groups' dynamical state, according to the optical data. The Table includes all groups for which a group centre could be reliably determined from the X-ray data.

For three out of the six listed groups (2PIGG\_s1520, 2PIGG\_s1571, 2PIGG\_n1320), the 2PIGG and X-ray centres coincide to within a few arc seconds. We furthermore note that for two of these three groups, namely 2PIGG\_s1520 and 2PIGG\_s1571, the 2PIGG centres coincide with the central galaxy. The group 2PIGG\_s1571 was classified in Paper I as a relaxed group, with the central galaxy identification indeed in agreement with both the 2PIGG-averaged centre and the peak of the X-ray emission. This group thus provides reassurance that, in well-behaved systems, the centre and central galaxy associations based on optical data are robust and physically-motivated.

Things can be trickier however for more complex structures. The group 2PIGG\_s1520 is classified as unrelaxed based on the optical data, but nevertheless there is a good agreement between the X-ray peak and the 2PIGG-averaged centre. On the other extreme, the group 2PIGG\_n1606 was classified as relaxed according to the optical data alone, but its diffuse emission is clearly double peaked, which is suggestive of a merger event. In 2PIGG\_n1606 the offset between the optical and X-ray centres as well as optical centre and central galaxy, is much larger than the separation between X-ray centre and central galaxy. This is consistent with the X-ray picture that the system is undergoing a merger, the system is unrelaxed, and the X-ray emission traces the largest of the merging structures. In the case of 2PIGG\_n1320, which is also an optically relaxed group, the galaxy corresponding to the peak of the X-ray emission is not the same as the optically-identified central galaxy of the group.

The remaining groups reported in Table 5 also show some degree of mismatch between the optical and X-ray centres. The group 2PIGG\_n1746, characterized by the smallest discrepancy, is classified as relaxed from the optical. 2PIGG\_n1746 is characterized by a mild separation between the 2PIGG and the X-ray centres, although the X-ray centre is closer to the central galaxy than to the optical centre. Therefore this group is also likely to be also dynamically unrelaxed in spite of the optical classification, as in the case of 2PIGG\_n1606 discussed above.

In the case of 2PIGG\_n1377, classified as dynamically unrelaxed, the separation between the optical and X-ray centre is mild, while the separation of either centre to the central galaxy is quite large.

These examples illustrate that there is a substantial difficulty in identifying group centres from optical data alone, and, most likely, also a substantial diversity in group properties and dynamical conditions. While the optical and X-ray data are often consistent, in several cases important discrepancies become apparent and complementary X-ray observations become important for a complete picture (see, also George et al. 2012). It is the combination of high quality optical data and X-ray observations that reveals subtle properties of the dynamical state of groups, which would be missed by an analysis based purely on either data set alone. This information is important in studies of galaxy properties and evolution as a function of group environment, which aim at establishing the physical processes and conditions responsible for triggering evolutionary mechanisms. Examples include structural and morphological properties as well as star formation and or AGN activity as a function of either the group-centric distance or the group dynamical conditions. It is obvious that mis-classifications of the group centre and/or dynamical state, introduce noise in the observed relations which can be amended with X-ray data. This straightforward comparison that we have conducted is therefore, above all, a strong warning of the relevance to have complementary X-ray information in order to establish the full dynamical picture of a galaxy group.

#### 4.2. $L_X$ vs $M$ Diagram and Mass Determinations

In the bottom left panel of Figure 3 we plot the group mass as a function of the X-ray luminosity from the diffuse intragroup medium. Data points with signal-to-noise better than two are shown for XMM-Newton and Chandra as blue circles and red pentagons, respectively. Data points with lower significance are also shown as upper limits for each respective instrument. Open and solid style indicates relaxed and unrelaxed systems, respectively, while horizontal bars correspond to statistical errors in the X-ray luminosity reported in Table 1 and 3. The group mass,  $M_{opt}$ , listed also in the above Tables, is provided by the ZENS catalog and is based on the optical luminosity of the group member galaxies. It is computed from the total optical luminosity of the group  $L_{Group}$ , using the mass-to-light ratio (see Eke et al. 2004; Carollo et al. 2013, for details)

$$\log(Y_{b_j}) = 2.28 + 0.4 \tanh\{1.9[\log(L_{Group}) - 10.6]\}. \quad (2)$$

The black open squares correspond to the group masses,  $M_{opt}$ , corrected for a selection bias as discussed in Sec. 3.3.

In order to compare with prediction from scaling relations, we also present in the same plot the black solid circles connected by a dash line. They indicate the position of the groups in the diagram if we derive their mass,  $M_X$ , from the X-ray luminosity using the  $L_X - M_X$  relation in Leauthaud et al. (2010). This relation is based on a joint analysis of X-ray and weak lensing of groups in COSMOS survey. The plot shows that our groups de-

part significantly from the scaling relation inferred from the X-ray selected groups. Except for 2PIGG\_s1571, our ZENS groups appear to be under-luminous for their stellar content. This is not surprising and accords to finding from previous studies (most recently Connolly et al. 2012, but see also discussion in the Introduction), which have shown that optically selected groups and clusters of galaxies tend to be less X-ray bright than X-ray selected ones. Corrections for the selection bias (open black squares) cannot account for the discrepancy.

The discrepancy is further illustrated in the middle-right panel, where the optical to X-ray mass ratio is plotted as a function of the X-ray mass,  $M_X$ . There is a clearly relative bias between the two estimates, with the optical masses being always larger than the X-ray masses (with a single exception represented by 2PIGG\_s1571). The discrepancy becomes significantly larger when the X-ray mass is compared to the dynamical mass (bottom right panel),  $M_{dyn}$ , determined from dynamical arguments (i.e. Connolly et al. 2012)

$$M_{dyn} = \frac{3\sigma_v^2 R_{200}}{G_N}, \quad (3)$$

indicating that the latter is a considerably less reliable mass proxy, due to large uncertainties mostly associated with the determination of velocity dispersions with respect to the group centre of mass from a few member galaxies.

The optical mass determinations ( $M_{opt}$ ) are usually thought to overestimate the actual mass of the group (see Sec. 4.2 below). In fact, the above bias is typically ascribed to the dynamical conditions of the group. However, in our limited sample there seems to be no indication that unrelaxed groups (solid symbols) are more under luminous than relaxed ones (open symbols). In addition, inspection of the individual group properties show that the under luminous groups span the full range in terms of bulge fraction of the central galaxy, which suggests that the under luminosity may not be simply related to a recent formation of the group. We have found, however, a slight correlation between the ratio of the optical to the X-ray mass, and the bulge fraction, in the sense that the discrepancy between the optical and X-ray masses seems to increase towards smaller bulge fraction. This suggests that the group stellar mass in the bulge component is a better proxy to the group mass than  $M_{opt}$  based on the total optical emission. This is supported by the results shown in the top-left panel of Fig. 3, where we multiply the ratio of the optical to X-ray group mass times the bulge fraction and plot it as a function of the X-ray mass. Compared to the plot of the original mass ratio in the middle-left panel of Fig. 3, the discrepancy between the two mass determinations appear significantly reduced, although not completely removed. Note that a similar results were also found in Andreon (2012), although at considerably larger mass scales. We have further found that, for the small sample of groups considered here, the above correction appears to be unbiased with respect to the different values of the bulge fraction. Even after the correction, however, the distribution of the X-ray luminosities with respect to the dash line remains asymmetric (see also Connolly et al. 2012), which may suggest that the under-luminous char-

acter of the observed ZENS groups may be genuine to some extent. However, the number of X-ray detections is currently too limited to draw any firm conclusion from the current data.

Note that, group 2PIGG\_s1571, which is detected with the best significance, departs from the scaling predictions in the opposite direction, i.e. is over-luminous by an order of magnitude. However, this could well be consistent with the observed large scatter in  $L_X$  at these mass scales (Eckmiller et al. 2012).

#### 4.3. Stellar Mass Fraction

In Fig. 4 we plot the stellar-to-total mass ratio as a function of the X-ray mass,  $M_X$ , where the total mass is  $M_X$ . The stellar mass is conventionally computed using galaxies with masses down to  $10^{10} M_\odot$  (?), where the ZENS catalogue is complete for any spectral type. Therefore, our values of the stellar mass fraction should be treated as lower limits. In Fig. 4 blue and red symbols indicate X-ray data from XMM-Newton and Chandra, respectively, while open and solid indicate relaxed and unrelaxed systems respectively. Only groups with X-ray detections with signal-to-noise better than two are shown, and upper limits are not plotted as they do not contribute additional information since they mostly crowd above the median values. The latter is indicated by a dashed line, which correspond to a value of 0.011.

The stellar fractions computed in the top panel are within 30% of the median value, except for 2PIGG\_s1571. The median of 0.011 is consistent with results obtained by Connelly et al. (2012) for optically selected groups and also Balogh et al. (2011) at similar sample size. Our fractions are lower than the values reported in Giodini et al. (2009), who however measured the stellar mass fraction within  $R_{500}$ , as opposed to the  $R_{200}$  as in our case, as well as Gonzales et al. (2007) who in addition took into account the contribution from intra-cluster light.

For comparison we also plot the stellar mass fraction contributed by the group most massive galaxy. It is indicated with a blue or red cross below the circle or pentagon symbol of the corresponding group. The plot shows that the most massive galaxy typically contains between 30 to 50 % of the total stellar mass fraction in the group.

#### 4.4. $L_X$ vs Global Galaxy Properties

As a first attempt to investigate whether either the diffuse X-ray emission or the galaxy properties or both show hints for a substantial interaction between the DIM and the group galaxies, we searched for correlations between the X-ray properties of the groups, i.e. their luminosity, and the general properties of the group member galaxies as a whole.

In Fig. 5 we show two examples of correlation that could in principle reveal such an effect. In the left panel of Fig. 5 for each group we plot the X-ray luminosity from the diffuse intragroup medium against the fraction of group galaxies with quiescent star formation. The star formation is determined for galaxies above the mass completeness limit of ZENS, i.e.,  $10^{10} M_\odot$ , and measured using photometric and spectroscopic measurements and proper correction for incompleteness (see Cibinel et al. 2013b, for details). In addition, in the right panel of

Fig. 5 the X-ray luminosity is plotted against the fraction of stellar mass of the group member galaxies that is locked in the bulge component. The latter is determined using the bulge-disk decomposition from both  $I$  and  $B$  band photometric data, again using galaxies with mass above  $10^{10} M_\odot$ . As in previous cases, in both figures data from XMM-Newton (blue circles) and Chandra (red pentagons) with signal-to-noise better than two are shown, together with upper limits for the respective instruments.

The  $L_X$  vs quenched fraction could contain information about the role of the DIM in quenching the star formation in group galaxies, while conversely the spheroid component, which correlates with black hole mass, could reveal impact of AGN activity on the DIM. However, we see no apparent correlation in either plot using the current data. The small size of the sample and the numerous upper limits compared to X-ray detections are clearly a limitation in this investigation, which argues for the acquisitions of X-ray data for a substantially larger sample. While it may sound tempting to employ a sample with significantly larger range in X-ray luminosity, it would in fact be much more useful to increase the sample size at fixed group halo mass, so to disentangle additional effects associated with group halo mass. A larger sample is also essential to separately investigate trends for central and satellite galaxy samples, and for satellites as a function of group-centric distance – both recognised key environmental parameters Weinmann et al. (2006, 2008); Carollo et al. (2013).

#### 5. CONCLUSIONS

We have conducted a pilot program of X-ray observations with the XMM-Newton and Chandra telescopes of a small subset of optically-selected groups belonging to the sample of 141 groups of the Zurich Environmental Study (ZENS). Observations with XMM-Newton were carried out for 8 groups during three observing cycles. With the addition of archival data for 4 groups, they amount to a total of 13 group observations. About one third of the data was lost due to flares. X-ray emission from the DIM was successfully detected for 6 groups, in addition to a marginal 1.8 sigma detection. The Chandra data were collected during Cycle 11. A total of 13 ZENS groups were observed and diffuse X-ray emission from the DIM was successfully detected above 2 sigmas for 4 groups.

The target groups have been selected to be in a narrow mass scale about  $10^{13} M_\odot$ , and at redshift  $z = 0.05 - 0.0585$ . The detections reveal a typical X-ray flux of in the energy band 0.5-2keV of  $\leq 10^{-14} \text{ erg cm}^{-2} \text{ s}^{-1}$ , which is one order of magnitude fainter than typical ROSAT groups (RASS). However, for many groups we were able to obtain only upper limits, indicating that despite uncertainties in the mass determination of the groups, our detections are likely probing the upper envelope of the X-ray emitting, optically selected ZENS groups.

The main results of this exploratory analysis can be summarized as follows:

- Small groups such as those probed by ZENS survey are characterized by large diversity properties and dynamical conditions. The X-ray data, in partic-

ular maps of the DIM, reveal features that would be missed by the analysis of the optical data alone. They thus provide important complementary information to optical data, which is necessary particularly for a robust classification of the dynamical conditions of the group.

- Our investigation of the X-ray luminosity versus group mass indicates that our optically selected ZENS groups may be under-luminous with respect to the prediction from scaling relations characterizing X-ray selected groups Leauthaud et al. (2010), as they crowd almost exclusively the space to the left of the  $M_X$  vs  $L_X$  line corresponding to the said scaling relation, the resulting asymmetry being even stronger than reported in Connolly et al. (2012).
- The mass determination based on the total optical luminosity of the groups is in better agreement with the mass determination based on X-ray emission than the dynamical mass estimates. The optical masses, however, remain always larger than the X-ray masses estimates, indicating the existence of a residual relative bias between the two mass proxies. There is tentative evidence that this discrepancy is reduced when the group mass determination is based on the luminosity of the bulge component of

the member galaxies, rather than the total luminosity (consistent with Andreon 2012, at larger mass scales). Note that the dynamical mass estimates could also be improved with refined determinations of the group member galaxies velocity dispersion as proposed recently in Erfanianfar et al. (2013).

- The group stellar mass fraction, obtained from the ratio of the groups total stellar mass and the total group mass determined from the X-ray emission, has a median value of 0.011. This is consistent with recent work of Connolly et al. (2012). The contribution to the stellar mass fraction from the most massive galaxies ranges between 30 to 50 %.

It is clear that the small number of diffuse X-ray measurements for  $\sim 10^{13} M_\odot$  groups limits at the moment our ability to robustly probe the effects of the interplay between the DIM and the member galaxies at this mass scale that is likely very relevant for environmentally-driven galactic evolution. This pilot program demonstrates however the potential return and importance of conducting a similar X-ray study on a group sample which is large enough to enable a statistically robust investigation of this crucial and yet unexplored issue in galaxy evolution.

## REFERENCES

- Andreon, S. 2012, *A&A*, 548, A83
- Balogh, M. L., Mazzotta, P., Bower, R. G., et al. 2011a, *MNRAS*, 412, 947
- Barnes, J. E. 1990, *Nature* 344, 379
- Barnes, J. E. 1990, *MNRAS* 333, 481
- Barnes, J. E., Hernquist, L. E. 1991, *ApJ*, 370, L65
- Bernet, M. L., Miniati, F., Lilly, S. J., Kronberg, P. P., Dessauges-Zavadsky, M., 2008, 454, 302
- Bernet, M. L., Miniati, F., Lilly, S. J. 2010, *ApJ*, 711, 380
- Bernet, M. L., Miniati, F., Lilly, S. J. 2012, *ApJ*, 761, 144
- Bielby et al. 2010, *A&A* 523, id.A66
- Borgani, S., Finoguenov, A., Kay, S. T., Ponman, T. J., Springel, V., Tozzi, P., Voit, G. M. 2005, *MNRAS*, 361, 233
- Bower, R. et al. 2006, *MNRAS* 370, 645
- Bower, R. et al. 2008, *MNRAS* 390, 1399
- Bruzual, G., & Charlot, S. 2003, *MNRAS*, 344, 1000
- Burns, J. O., et al. 1996, *ApJ*, 467, L49
- Cappelluti N., Ranalli P., Roncarelli M., et al., 2012, *MNRAS*, 427, 651
- Carollo, C. M., Cibinel, A., Lilly, S. J., Miniati, F., Norberg, P., Silverman, J. D., van Gorkom, J., Cameron, E., Finoguenov, A., Pipino, A., Rudick, C. S., Lu, T., Peng, Y. 2013, *ApJ*, 776, 71
- Carollo, C. M., Cibinel, A., Lilly, S. J., et al. 2014, *arXiv:1402.1172*
- Cavaliere, A., Menci, N., Tozzi, P. 1998, *ApJ*, 501, 493
- Cibinel, A., Carollo, C. M., Lilly, S. J., Miniati, F., Silverman, J. D., van Gorkom, J. H., Cameron, E., Finoguenov, A., Norberg, P., Pipino, A., Rudick, C. S., Lu, T., Peng, Y. 2013a, *ApJ*, 776, 72
- Cibinel, A., Carollo, C. M., Lilly, S. J., Bonoli, S., Miniati, F., Pipino, A., Silverman, J. D., van Gorkom, J. H., Cameron, E., Finoguenov, A., Norberg, P., Rudick, C. S., Lu, T., Peng, Y. 2013, *ApJ* 777, 116
- Colless, et al. 2001, *MNRAS* 328, 1039
- Connolly, J. L., et al. 2012, *ApJ* 756, 139
- Croton, D. et al. 2006, *MNRAS* 367, 864
- Donahue, M. et al. 2002, *ApJ* 569, 689
- Ebeling, H., Voges, W., Böhringer, H. 1994, *ApJ*, 436, 44
- Ekcmiller, H. J., Hudson, D. S., Reiprich T. H. 2012, *A&A*, 535, A105
- Eke, V. et al 2004, *MNRAS* 348, 886
- Eke, V. et al. 2005, *MNRAS* 362, 1233
- Erfanianfar, V. et al. 2013, *ApJ* 765, 117
- Feldmann, R., Carollo, C. M., Mayer, L., et al. 2010, *ApJ*, 709, 218
- Finoguenov, A., Arnaud, M., David, L. P. 2001, *ApJ*, 555, 191
- Finoguenov, A., Guzzo L., Hasinger G., et al. 2007, *ApJS* 172, 182
- Finoguenov, A., Connolly J. L., Parker L. C., et al. 2009, *ApJ* 704, 564
- Finoguenov A., Watson M. G., Tanaka M., et al., 2010, *MNRAS*, 403, 2063
- Fukugita, M., Hogan, C. J., Peebles, P. J. E. 1998, *ApJ*, 503, 518
- George M. R., Leauthaud A., Bundy K., et al., 2012, *ApJ*, 757, 2
- Gilbank, D. G., Bower, R. G., Castander, F. J., Ziegler, B. L., 2004, *MNRAS*, 348, 551
- Giodini, et al. 2010, *ApJ*, 714, 218
- Giodini, S., Pierini, D., Finoguenov, A., et al. 2009, *ApJ*, 703, 982
- Giodini, S., Finoguenov, A., Pierini, D., et al. 2012, *A&A*, 538, A104
- Gonzalez, A. H., Zaritsky, D., & Zabludoff, A. I. 2007, *ApJ*, 666, 147
- Häring, R. & Rix, H.W. 2004, *ApJ* 604, L89
- Heldson, S. F., Ponman, T. J. 2000, *MNRAS*, 315, 356
- Hickox R. C., Markevitch M., 2006, *ApJ*, 645, 95
- Jeltema, T., et al., 2009, *MNRAS* in press
- Kawata, D. & Mulchaey, J. 2008, *ApJ* 672, L103
- Knobel, C. et al. 2009, *ApJ* 697, 1842
- Knobel, C., Lilly, S. J., Kovac, K., et al. 2012, *arXiv:1211.5607*
- Komatsu, E., Dunkley, J., Nolte, M. R., Bennett, C. L., Gold, B., Hinshaw, G., Jarosik, N., Larson, D., Limon, M., Page, L., Spergel, D. N., Halpern, M., Hill, R. S., Kogut, A., Meyer, S. S., Tucker, G. S., Weiland, J. L., Wollack, E., & Wright, E. L. 2009, *ApJS*, 180, 330
- Leauthaud, A. et al. 2010, *ApJ*, 709, 97
- Lloyd-Davis, E. J., Ponman, T. J., Cannon, D. B. 2000, *MNRAS*, 315, 689
- Lubin, L. M., Mulchaey, J. S., Ponman, T. J. 2004, *ApJ*, 601, L9
- Magorrian, J. et al. 1998, *AJ*, 115 2285
- Mahdavi, A., Böhringer, H., Geller, M. J., Ramella, M. 1997, *ApJ*, 483, 68
- Mahdavi, A., Böhringer, H., Geller, M. J., Ramella, M. 2000, *ApJ*, 534, 114



- Madhavi, A., Finoguenov, A., Böhringer, H., Geller, M. J., Henry, J. P., *ApJ*, 622, 187
- Mayer, L. et al. 2001 *ApJ* 559, 754
- McCarthy, I.G. et al. 2008, *MNRAS* 386, 1309
- McCarthy, I.G. et al. 2010, *MNRAS* 406, 822
- McIntosh, D. H., Guo, Y., Hertzberg, J., et al. 2008, *MNRAS*, 388, 1537
- McGee, S. L., Balogh, M. L., Wilman, D. J., et al. 2011, *MNRAS*, 413, 996
- Mihos, C. 2003, *Carnegie Observatories Astrophysics Series*, Vol. 3: Clusters of Galaxies: Probes of Cosmological Structure and Galaxy Evolution, ed. J. S. Mulchaey, A. Dressler, A. Oemler (Cambridge: Cambridge Univ. Press), 2003.
- Moore, B., Lake, G., Katz, N. 1998, *ApJ*, 495, 139
- Mulchaey, J. *ARA&A*, 2000, 38, 289
- Mulchaey, J., Davis, D. S., Mushotzky, R. F., Burstein, D. 2003, *ApJ*, 145, 39
- Oesch, P. A., Carollo, C. M., Feldmann, R., et al. 2010, *ApJ*, 714, L47
- Osmond, J. P. F., Ponman, T. J. 2004, *MNRAS*, 350, 1511
- O’Sullivan, E., Kolokythas, K., Raychaudhury, S., Vrtilak, J. M., & Kantharia, N. 2014, *arXiv:1402.4676*
- Paturel, G., Petit, C., Prugniel, P., et al. 2003, *A&A*, 412, 45
- Peng, Y.-j., Lilly, S. J., Renzini, A., & Carollo, M. 2012, *ApJ*, 757, 4
- Poggianti, B. M., Desai, V., Finn, R., et al. 2008, *ApJ*, 684, 888
- Ponman, T. J., Bourner, P. D. J., Ebeling, H., Böhringer, H. 1996, *MNRAS*, 283, 690
- Ponman, T. J., Cannon, D. B., Navarro, J. F. 1999, *Nature*, 397, 135
- Ponman, T. J., Sanderson, A. J. R., Finoguenov, A. 2003, *MNRAS*, 343, 331
- Popesso, P., Biviano, A., Böhringer, H., Romaniello, M. 2007, *A&A*, 461, 397
- Prat, G. W., et al. 2010, *A&A*, 511, A85
- Rasmussen, J., Ponman, T. J., Mulchaey, J. S., Miles, T. A., Raychaudhury, S. 2006, *MNRAS* 373, 653
- Rasmussen, J., Ponman, T. J., 2007, *MNRAS*, 380, 1554
- Rasmussen, J., Ponman, T. J., 2009, *MNRAS*, 399, 239
- Robotham, A. S. G., Liske, J., Driver, S. P., et al. 2013, *MNRAS*, 431, 167
- Silverman, J. D., Miniati, F., Finoguenov, A., Carollo, C. M., Cibinel, A., Lilly, S. J., Schawinski, K. 2014, *ApJ* 780, 67
- Skibba, R. A. 2009, *MNRAS*, 392, 1467
- Skrutskie, M. F., Cutri, R. M., Stiening, R., et al. 2006, *AJ*, 131, 1163
- Tal, T., Dekel, A., Oesch, P., et al. 2014, *arXiv:1401.2984*
- Tanaka M., Finoguenov A., Mirkazemi M., et al., 2012b, *ArXiv e-prints*
- Vikhlinin A., McNamara B. R., Forman W., Jones C., Quintana H., Hornstrup A., 1998, *ApJ*, 502, 558
- Vikhlinin A., Kravtsov A., Forman W., et al., 2006, *ApJ*, 640, 691
- Vikhlinin, A., Burenin, R. A., Ebeling, H., et al. 2009, *ApJ*, 692, 1033
- van den Bosch, F. C., Aquino, D., Yang, X., Mo, H. J., Pasquali, A., McIntosh, D. H., Weinmann, S. M., & Kang, X. 2008, *MNRAS*, 387, 79
- Voit, G. M., Kay, S. T., Bryan, G. L. 2005, *MNRAS*, 364, 909
- Weinmann, S. et al. 2006, *MNRAS*, 372, 1161
- Weinmann, S. et al. 2008, *MNRAS*, 394, 1213
- Weinmann, S. M., Kauffmann, G., van den Bosch, F. C., Pasquali, A., McIntosh, D. H., Mo, H., Yang, X., & Guo, Y. 2009, *MNRAS*, 394, 1213
- Wetzel, A. R., Tinker, J. L., Conroy, C., & van den Bosch, F. C. 2013, *MNRAS*, 432, 336
- York, D. et al 2000, *AJ*, 120, 1579
- Zabludoff, A. & Mulchaey 1998, *AJ*, 496, .39

TABLE 1  
XMM-Newton's LOG OF ZENS GALAXY GROUP OBSERVATIONS

Target	OBS ID	RA (J2000)	DEC (J2000)	Redshift	# of galaxies	$M_{Group}$ ( $10^{13} M_{\odot}$ )	Cicle	Exp (ksec)	Note <sup>a</sup>
2PIGG_s1520	0655300101	00:02:01.79	-34:52:55.5	0.05434	9	1.55	AO-9	33.0	
2PIGG_s1571	0655300301	02:37:04.33	-25:23:34.3	0.0568	10	1.52	AO-9	38.8	
2PIGG_s1783	0655300601	22:17:26.33	-36:59:48.1	0.05833	8	4.90	AO-9	39.4	
2PIGG_s1614	0674480301	22:25:15.88	-25 23 15.4	0.05676	18	4.98	AO-10	15.5	F
2PIGG_s1471	0674480901	23:45:01.81	-26:37:26.8	0.05276	15	3.91	AO-10	13.0	
2PIGG_n1466	0674480401	14:04:01.63	-01:40:06.9	0.05292	17	4.980	AO-10	15.0	F
2PIGG_n1572	0674480701	14:25:33.40	-01:30:00.4	0.05501	19	4.72	AO-10	15.0	
2PIGG_s1799	0693741001	01:14:34.43	-33:56:09.8	0.05819	13	3.35	AO-11	25.0	F
2PIGG_n1606	0693741601	10:38:36.50	+01:46:01.2	0.056	7	1.55	AO-11	25.7	
2PIGG_n1714	0150870401	10:36:06.57	-04:02:11.8	0.0576	7	2.00	AO-2	32.5	A
2PIGG_n1377	0207060301	11:32:42.10	-03:50:20.0	0.05154	23	7.51	AO-3	27.7	A,F
2PIGG_n1330	0305800101	10:27:36.72	-03:03:58.8	0.05044	5	1.02	AO-4	24.9	A
2PIGG_s1783	0550460801	22:17:26.33	-36:59:48.1	0.05833	8	4.90	AO-7	28.0	A

<sup>a</sup> F=flared, A=Archival Data

TABLE 2  
XMM-Newton DATA ON DIFFUSE INTRAGROUP EMISSION

Target	Total cnts	Bkgd cnts	Point src	Rad (')	$L_x^a$ ( $10^{41}$ erg/s)	$M_{200}$ ( $10^{13} M_{\odot}$ )	R200 (deg)	$T_x$ (keV)	Flux <sup>b</sup> ( $10^{-14}$ erg/s/cm <sup>2</sup> )	S/N
2PIGG_s1520	4707±69	3576	608	3.3	3.38±0.50	1.29±0.11	0.126	0.44±0.02	(3.10±0.46)	6.77
2PIGG_s1571	16938±130	8534	1630	4.9	31.9±0.68	4.96±0.06	0.189	0.90±0.01	(27.88±0.59)	46.87
2PIGG_s1783	8564±92	5137	2957	4.0	2.28±0.45	1.02±0.12	0.109	0.40±0.02	(1.75±0.35)	5.04
2PIGG_s1614	2426±49	2294	50	5.0	3.10±1.70	1.23±0.37	0.119	0.43±0.05	(2.57±1.41)	1.82 <sup>c</sup>
2PIGG_s1471	3235±57	2518	607	5.0	1.75±0.82	0.87±0.23	0.114	0.38±0.04	(1.63±0.76)	2.13 <sup>c</sup>
2PIGG_n1572	3998±63	3650	377	5.0	<1.69±0.85	<0.85±0.24	<0.109	<0.37±0.04	<(1.43±0.72)	-0.93 <sup>d</sup>
2PIGG_s1799	4367±66	4014	78	4.0	<7.34±1.77	<2.05±0.28	<0.138	<0.55±0.04	<(6.08±1.47)	4.13 <sup>e</sup>
2PIGG_n1606	1558±39	910	411	2.4	2.34±0.40	1.03±0.10	0.113	0.40±0.02	(1.95±0.34)	5.80
2PIGG_n1377	328±18	232	14	1.5	6.26±1.44	1.87±0.25	0.150	0.52±0.03	(6.64±1.53)	4.35

<sup>a</sup> 0.1-2.4keV

<sup>b</sup> 0.5-2keV

<sup>c</sup> A 2 sigma detection

<sup>d</sup> A 2 sigma-limit is calculated

<sup>e</sup> Upper limit

TABLE 3  
Chandra's LOG OF ZENS GALAXY GROUP OBSERVATIONS

Target	OBS ID	RA (J2000)	DEC (J2000)	Redshift	# of galaxies	$M_{Group}$ ( $10^{13} M_{\odot}$ )	Cicle	Exp (ksec)	Note
2PIGG_s1571	11613	02:37:04.33	-25:23:34.3	0.0568	10	1.52	11	10.06	
2PIGG_n1610	11617-11620	09:53:38.23	-05:08:21.4	0.0562	10	1.45	11	10.03	
2PIGG_n1702	11621-11624	09:54:30.67	-04:06:03.3	0.0574	9	2.26	11	9.88	
2PIGG_n1347	11625, 11627	09:59:44.62	-05:16:52.6	0.0521	10	2.90	11	10.29	
2PIGG_n1480	11629, 11631	10:15:31.91	-05:37:06.9	0.0537	13	2.26	11	9.97	
2PIGG_n1320	11633-11636	10:17:55.04	-01:22:53.4	0.0508	10	3.00	11	10.05	
2PIGG_n1441	11637, 11639	11:18:10.68	-04:27:36.1	0.0531	15	3.41	11	9.97	
2PIGG_n1381	11641, 11643, 11644	14:28:12.53	-02:31:12.4	0.0522	10	1.22	11	10.16	
2PIGG_n1598	11645	14:35:54.08	-01:16:42.7	0.0560	9	2.67	11	9.79	
2PIGG_n1746	11649, 11652	14:40:20.07	-03:45:56.2	0.0585	9	1.65	11	10.18	
2PIGG_s1752	11653, 11655	22:21:10.68	-26:00:24.6	0.0577	11	5.60	11	10.35	
2PIGG_s1671	11657-11660	22:24:00.14	-30:00:17.9	0.0567	10	2.83	11	10.58	

TABLE 4  
*Chandra* DATA ON DIFFUSE INTRAGROUP EMISSION

Target	Total cnts	Bkdg cnts	Point src	Rad (')	$L_x^a$ ( $10^{41}$ erg/s)	$M_{200}$ ( $10^{13} M_\odot$ )	$R_{200}$ (deg)	$T_x$ (keV)	Flux <sup>b</sup> ( $10^{-14}$ erg/s/cm <sup>2</sup> )	S/N
2PIGG_s1571	616±24.8	332	17	3	34.33±3.19	5.19±0.28	0.19	0.93±0.03	30.0±2.79	10.76
2PIGG_n1610	185±13.6	179	28.9	2	<3.72±1.86	<1.37±0.24			<3.20±1.60	-1.68
2PIGG_n1702	86.9±9.3	65	0	1.5	2.84±1.26	1.16±0.24	0.12	0.42±0.04	2.29±1.02	2.26
2PIGG_n1347	194±13.9	133	34.6	2	<3.26±1.63	<1.27±0.35			<3.24±1.62	1.90
2PIGG_n1480	157±12.5	151	7.6	2	<3.07±1.54	<1.22±0.34			<2.86±1.43	-0.13
2PIGG_n1320	133±11.5	68	14.7	1.4	5.39±1.24	1.71±0.23	0.15	0.50±0.03	5.86±1.34	4.36
2PIGG_n1441	199±14.1	155	20.1	2	<3.46±1.73	<1.31±0.36			<3.32±1.66	1.70
2PIGG_n1381	208±14.4	159	37.8	2	<3.18±1.59	<1.25±0.34			<3.16±1.58	0.78
2PIGG_n1598	184±13.6	141	23.7	2	<3.69±1.84	<1.36±0.37			<3.19±1.60	1.42
2PIGG_n1746	62±7.9	31	0	0.9	5.08±1.29	1.65±0.24	0.13	0.49±0.03	4.09±1.04	3.92
2PIGG_s1752	374±19.3	372	16	3	<5.16±2.58	<1.66±0.46			<4.27±2.14	-0.72
2PIGG_s1671	438±20.9	391	27	3	<5.36±2.68	<1.70±0.47			<4.62±2.31	0.96

<sup>a</sup> 0.1-2.4keV

<sup>b</sup> 0.5-2keV

TABLE 5  
OPTICAL VS X-RAY CENTERS

Group	RA (J2000)	DEC (J2000)	$\Delta\alpha_{\text{Opt-Xray}}$ (")	$\Delta\alpha_{\text{Opt-CG}}$ (")	$\Delta\alpha_{\text{CG-Xray}}$ (")	State <sup>a</sup>
2PIGG_s1520	00:02:01.79	-34:52:55.5	3.3	0.23	3.3	U
2PIGG_s1571	02:37:04.33	-25:23:34.3	7.4	0.24	7.3	R
2PIGG_n1377	11:32:42.10	-03:50:20.0	60	718	695	U
2PIGG_n1320	10:17:55.04	-01:22:53.4	1.8	312	310	R
2PIGG_n1746	14:40:20.07	-03:45:56.2	36	38	10	R
2PIGG_n1606	10:38:36.50	01:46:01.2	280	268	36	R

<sup>a</sup> R=relaxed, U=unrelaxed

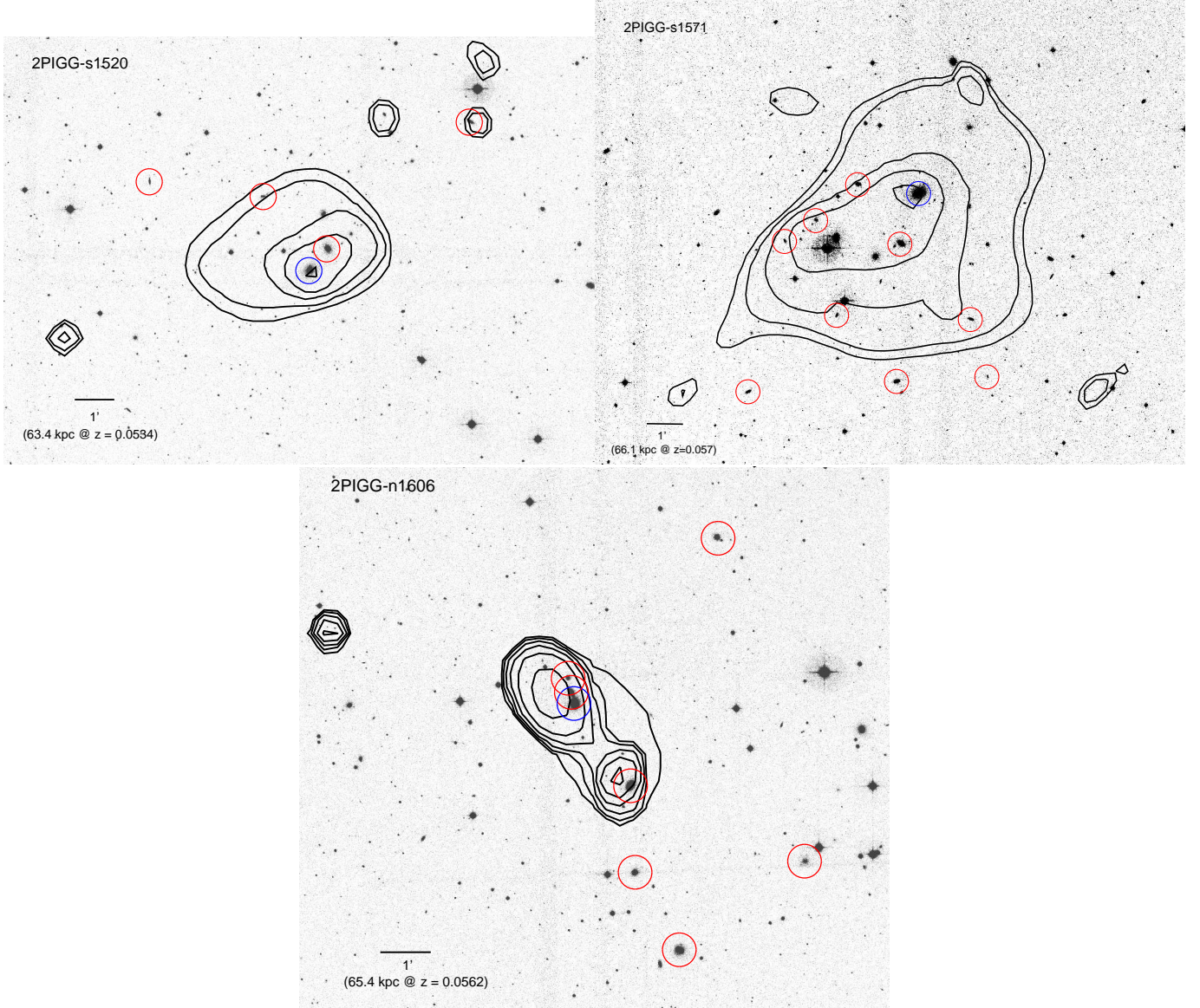


FIG. 1.— XMM-Newton measurement of the Diffuse Intragroup Medium X-ray emission from the ZENS groups 2PIGG\_s1520 (top) 2PIGG\_s1571 (centre) and 2PIGG\_n1606 (bottom), overlaid with optical i band image. Black contours indicate the surface brightness level of X-ray emission on a log scale. Red circles mark the galaxy members and the those in blue the central galaxy determined prior to knowledge of the X-ray emission.

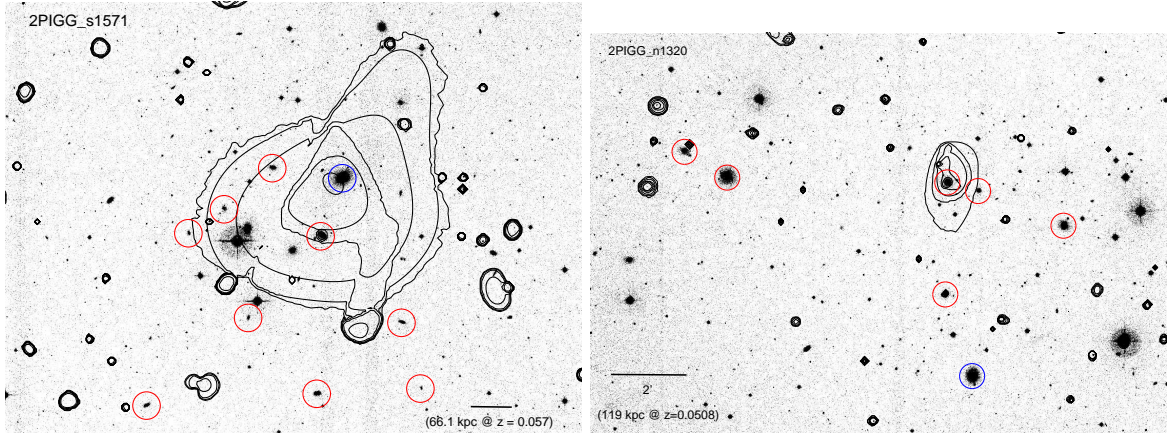


FIG. 2.— Chandra measurements of the Diffuse Intragroup Medium X-ray emission from the ZENS groups 2PIGG\_s1571 (top) and 2PIGG\_n1320 (bottom), overlaid with optical i band image. Black contours indicate the surface brightness level of X-ray emission on a log scale. Red circles mark the galaxy members and the those in blue the central galaxy determined prior to knowledge of the X-ray emission.

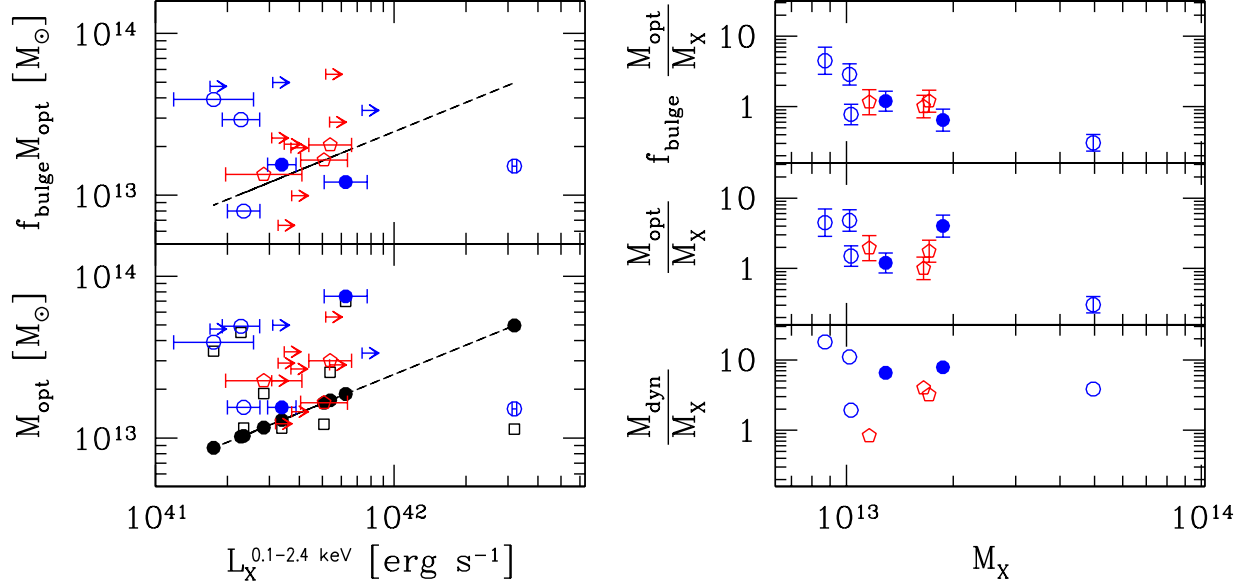


FIG. 3.— *Left:* Group mass versus X-ray luminosity from the diffuse intragroup medium. Measurements from XMM-Newton (blue circles) and Chandra (red pentagons) with signal-to-noise better than two are shown together with upper limits for the respective instruments. Open and solid symbols denote relaxed and unrelaxed system, respectively. Horizontal bars correspond to statistical errors in the X-ray luminosity as reported in Table 1 and 3. The group mass for the ZENS sample is obtained from the groups optical luminosity and is given in the same Tables. For comparison, the black solid circles connected by a dash line indicate the position of the groups in the diagram if their mass is derived from the X-ray luminosity using the  $L_X - M_X$  relation established from the joint analysis of X-ray and weak lensing for groups in COSMOS (Leauthaud et al. 2010). The black open squares are the optically determined groups masses,  $M_{\text{opt}}$ , corrected for a selection bias as discussed in Sec. 3.3. *Right:* dynamical (bottom), optical (middle) and bulge-based optical ( $\equiv f_{\text{bulge}} \times M_{\text{opt}}$ ) group mass estimates divided by the X-ray mass. Data from XMM-Newton (blue circles) and Chandra (red pentagons) with signal-to-noise better than two are shown. Open and solid indicate relaxed and unrelaxed systems respectively. Error bars include errors associated with X-ray mass determination reported in Table 2 and 4, and 30% mass estimate for the optical mass (see Carollo et al. 2013).

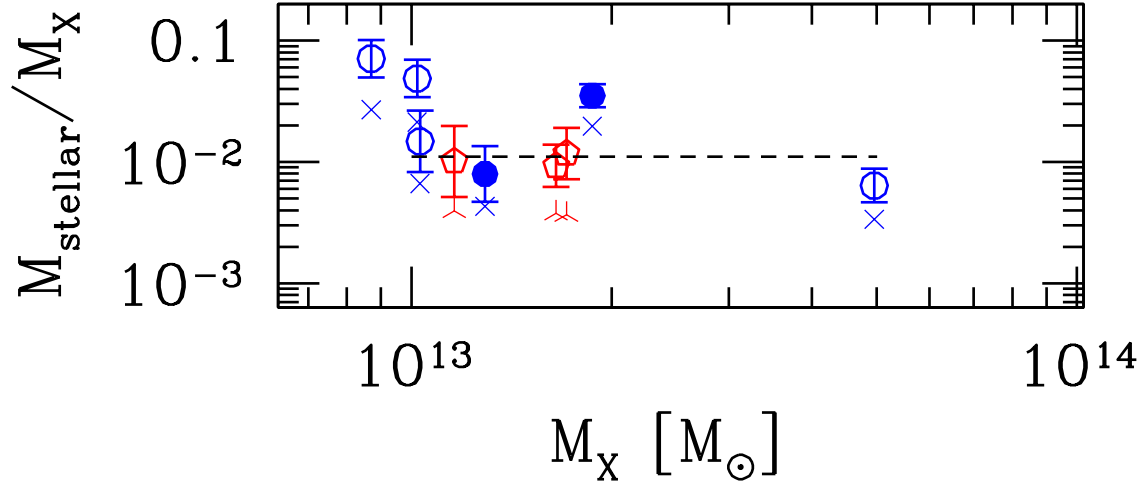


FIG. 4.— Stellar-to-total mass ratio as a function of the X-ray mass, where the total mass is the X-ray mass obtained using the scaling relations in Leauthaud et al. (2010). Blue and red symbols indicate X-ray data from XMM-Newton and Chandra, respectively, while open and solid indicate relaxed and unrelaxed systems respectively. The dash line indicate the median value of 0.011. Only groups with X-ray detections with signal-to-noise better than two are shown. Upper limits do not contribute additional information as they mostly crowd above the median bar of the top panel. Error bars include errors associated with X-ray mass determination reported in Table 2 and 4, and errors based on the upper limits of the best stellar mass estimate given in Carollo et al. (2013).

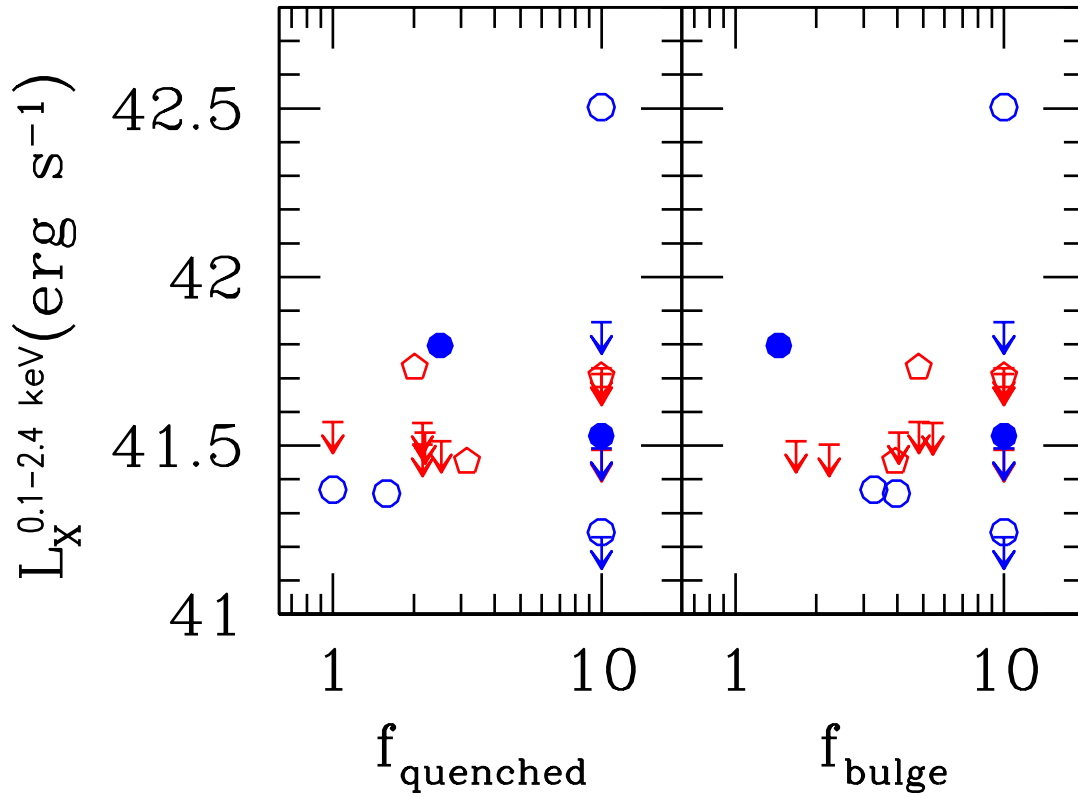


FIG. 5.— Group X-ray luminosity as a function of the fraction of group galaxies with quiescent star formation (left) and the fraction of bulge stellar mass of the group member galaxies (right). Quantities are computed from galaxies with mass above  $10^{10} M_{\odot}$ , where the ZENS catalogue is complete. The star formation for individual galaxies is determined through photometric and spectroscopic measurements and proper correction for incompleteness; the bulge component is determined using a bulge-disk decomposition based on both I and B band photometric data (Cibinel et al. 2013b). Data from *XMM-Newton* (blue circles) and *Chandra* (red pentagons) with signal-to-noise better than two are shown together with upper limits for the respective instruments. Open and solid indicate relaxed and unrelaxed systems respectively.